

# A Metric for Three-Dimensional Color Discrimination Derived from V1 Population Fisher Information

Michael Menke

## Abstract

We derive a Riemannian metric on three-dimensional color space from the Fisher information of neural population codes in the visual pathway. Photoreceptor adaptation, retinal opponent channels, and cortical population encoding each map onto a geometric construction, producing a metric tensor whose components correspond to measurable neural quantities. The resulting 17-parameter model is fitted jointly to four independent threshold datasets: MacAdam’s (1942) chromaticity ellipses, the Koenderink et al. (2026) three-dimensional ellipsoids, Wright’s (1941) wavelength discrimination function, and the Huang et al. (2012) threshold color difference ellipses, covering 96 independently measured discrimination conditions across varied chromaticities and luminances. The joint fit achieves STRESS of 23.9 on MacAdam, 20.8 on Koenderink et al., 30.1 on Wright, and 30.8 on Huang et al.

## 1 Introduction

Defining a perceptually meaningful metric on color space has been a central problem in color science since Helmholtz [9] proposed a Riemannian metric based on Weber’s law. Subsequent proposals by Schrödinger [29] and Stiles [31] refined the metric but could not accommodate later empirical data. MacAdam’s [25] measurements of chromatic discrimination ellipses shifted the field from theoretical metrics to empirical characterization, establishing that perceptual color space is locally anisotropic and spatially inhomogeneous. Modern color difference formulas such as CIEDE2000 [23] represent decades of empirical refinement but remain parametric corrections layered onto a pre-existing coordinate system.

Here we take a different approach: we derive the discrimination metric from the Fisher information of a population of chromatically tuned V1 neurons. Each component of the metric tensor traces to a specific neural population with a specific noise model and transduction function, and each free parameter corresponds to a quantity constrained by neurophysiology. Two cross-channel normalization mechanisms, koniocellular suppression by L-M opponent activity and S-cone disinhibition of the non-cardinal population, provide chromaticity-dependent gain control that resolves tradeoffs between near-white and spectrum-locus chromaticities. The model is validated against four independent psychophysical datasets spanning chromaticity ellipses, three-dimensional ellipsoids, monochromatic wavelength discrimination, and threshold colour differences at varied chromaticities and luminances.

## 2 Photoreceptor Adaptation

### 2.1 Cone excitations

A color stimulus with CIE 1931 tristimulus values  $(X, Y, Z)$  produces cone excitations via the Smith–Pokorny [30] transformation, based on the cone spectral sensitivities of Bowmaker & Dartnall [1]:

$$\begin{pmatrix} L \\ M \\ S \end{pmatrix} = M_{\text{SP}} \begin{pmatrix} X \\ Y \\ Z \end{pmatrix}, \quad M_{\text{SP}} = \begin{pmatrix} 0.15514 & 0.54312 & -0.03286 \\ -0.15514 & 0.45684 & 0.03286 \\ 0 & 0 & 0.01608 \end{pmatrix}. \quad (1)$$

### 2.2 Von Kries adaptation

Chromatic adaptation is modeled by independent gain control on each cone class [33]:

$$L_a = L/L_W, \quad M_a = M/M_W, \quad S_a = S/S_W, \quad (2)$$

where  $(L_W, M_W, S_W)$  are the cone excitations of the adaptation illuminant at a reference luminance  $Y_{\text{ref}}$ . This multiplicative normalization is supported by the physiology of cone photoreceptor gain control [28] and by psychophysical evidence for the approximate validity of von Kries adaptation [2]. The adapted signals are dimensionless ratios centered at unity for the adaptation white:  $L_a(\text{white}) = M_a(\text{white}) = S_a(\text{white}) = 1$ .

## 3 Opponent Channel Formation

### 3.1 Parvocellular coordinate

The midget ganglion cells of the primate retina compute L versus M opponency [6, 16]. Weber’s law ( $\Delta L/L \approx \text{const}$ ; [11]) implies that the coordinate rendering equal stimulus steps into equal perceptual distances is the logarithm of the L/M ratio. However, midget cells also exhibit contrast gain control [16], and their response saturates at high chromatic contrasts. To capture both the near-neutral Weber regime and the saturation at extreme chromaticities, we pass the log-ratio through a Naka–Rushton [27] compressive nonlinearity:

$$u = \log(L_a/M_a), \quad z = z_{\text{max}} \text{sign}(u) \frac{|u|^{p_z}}{|u|^{p_z} + \kappa_z}, \quad (3)$$

where  $z_{\text{max}}$  is the saturation ceiling,  $p_z$  controls the shape of the compression, and  $\kappa_z$  is the half-saturation constant. Near the adaptation white ( $|u| \ll \kappa_z^{1/p_z}$ ), the coordinate reduces to  $z \approx (z_{\text{max}}/\kappa_z) u$ , recovering Weber’s law with effective gain  $z_{\text{max}}/\kappa_z$ . At extreme chromaticities ( $|u| \gg \kappa_z^{1/p_z}$ ),  $z$  saturates toward  $\pm z_{\text{max}}$ . This parallels the Naka–Rushton nonlinearity applied to the koniocellular channel (Section 3.2) and treats both opponent pathways symmetrically.

**Proposition 3.1.** *The coordinate  $z$  depends only on chromaticity, not on luminance. That is, changing  $Y$  at fixed  $(x, y)$  leaves  $z$  unchanged.*

*Proof.* At fixed chromaticity  $(x, y)$ , the tristimulus values  $(X, Y, Z)$  are proportional to  $Y$ :  $X = Yx/y$ ,  $Z = Y(1 - x - y)/y$ . Since  $M_{\text{SP}}$  is linear, all cone signals scale by the same factor  $Y'/Y$  under a luminance change. This common factor cancels in the ratio  $L_a/M_a$ , leaving  $z$  unchanged. The same argument applies to  $r = S_a/(L_a + M_a)$  and therefore to  $w$ .  $\square$

### 3.2 Koniocellular coordinate

The small bistratified ganglion cells compute S versus  $(L+M)$  opponency [5]. The relevant signal is the ratio

$$r = S_a / (L_a + M_a), \quad (4)$$

which is also luminance-invariant by the same argument. At the adaptation white,  $r = 1/(1+1) = 0.5$ .

This ratio is passed through a Naka–Rushton [27] compressive nonlinearity:

$$w = \frac{r^{p_s}}{r^{p_s} + \kappa_s}, \quad (5)$$

modeling the saturation of the koniocellular pathway’s contrast-response function [32]. The function  $w: \mathbb{R}^+ \rightarrow (0, 1)$  is monotonically increasing, with  $w \rightarrow 0$  as  $r \rightarrow 0$  and  $w \rightarrow 1$  as  $r \rightarrow \infty$ .

*Remark 3.2.* The parvocellular channel compresses  $\log(L_a/M_a)$ ; the koniocellular channel compresses  $S_a/(L_a + M_a)$ . The two pathways retain different exponents and half-saturation constants, reflecting the genuine physiological differences between them: the parvocellular pathway ( $\sim 80\%$  of LGN neurons) has higher contrast gain and broader dynamic range [16], while the koniocellular pathway ( $\sim 10\%$  of LGN neurons) has narrower dynamic range and stronger compressive nonlinearity [10, 32].

## 4 Cortical Population Fisher Information

### 4.1 Fisher information for a single Poisson neuron

The link between neural encoding and Riemannian geometry is Fisher information. Consider a single neuron whose spike count  $r$  on a given trial is drawn from a Poisson distribution with mean firing rate  $f(\mathbf{s})$ , where  $\mathbf{s} = (s_1, s_2)$  is a two-dimensional stimulus (here, the opponent coordinates  $(z, w)$ ). The Poisson probability of observing  $r$  spikes is  $P(r) = f^r e^{-f}/r!$ , so the log-likelihood is

$$\ell = r \log f(\mathbf{s}) - f(\mathbf{s}) - \log(r!).$$

The Fisher information matrix is defined as the expected negative Hessian of the log-likelihood:

$$I_{ij}(\mathbf{s}) = -\mathbb{E} \left[ \frac{\partial^2 \ell}{\partial s_i \partial s_j} \right].$$

To evaluate this for the Poisson case, we compute the derivatives of  $\ell$ . The first partial derivative is

$$\frac{\partial \ell}{\partial s_i} = \frac{r}{f} \frac{\partial f}{\partial s_i} - \frac{\partial f}{\partial s_i} = \left( \frac{r}{f} - 1 \right) \frac{\partial f}{\partial s_i}.$$

Differentiating again,

$$\frac{\partial^2 \ell}{\partial s_i \partial s_j} = -\frac{r}{f^2} \frac{\partial f}{\partial s_i} \frac{\partial f}{\partial s_j} + \left( \frac{r}{f} - 1 \right) \frac{\partial^2 f}{\partial s_i \partial s_j}.$$

Taking the expectation with  $\mathbb{E}[r] = f$ , the second term vanishes (since  $\mathbb{E}[r/f - 1] = 0$ ), leaving

$$I_{ij}(\mathbf{s}) = -\mathbb{E} \left[ \frac{\partial^2 \ell}{\partial s_i \partial s_j} \right] = \frac{1}{f(\mathbf{s})} \frac{\partial f}{\partial s_i} \frac{\partial f}{\partial s_j}. \quad (6)$$

In matrix form,  $I = f^{-1} \nabla f \nabla f^T$ , where  $\nabla f = (\partial f / \partial s_1, \partial f / \partial s_2)^T$ . The Poisson Fisher information depends only on the tuning curve  $f(\mathbf{s})$  and its gradient; higher-order properties of the spike count distribution do not enter.

## 4.2 From Fisher information to discrimination ellipsoids

The Fisher information matrix is the natural metric tensor for discrimination because it determines the smallest detectable stimulus change. To see why, consider an observer who must estimate the stimulus  $\mathbf{s}$  from the spike counts of a neural population. Any estimator  $\hat{\mathbf{s}}$  will fluctuate from trial to trial due to the randomness of spiking. The covariance matrix  $\text{Cov}[\hat{\mathbf{s}}]$  describes the shape and size of these fluctuations: its diagonal entries are the variances of each coordinate estimate, its off-diagonal entries capture correlations between estimation errors, and its eigenvectors define the directions in stimulus space along which the estimate is most and least precise.

The Cramér–Rao inequality [4] places a lower bound on these fluctuations. For any unbiased estimator,

$$\text{Cov}[\hat{\mathbf{s}}] \succeq I(\mathbf{s})^{-1}, \quad (7)$$

where  $\succeq$  denotes the positive semi-definite ordering, meaning  $\text{Cov} - I^{-1}$  has no negative eigenvalues. In words: no estimation strategy can reduce the trial-to-trial variability below  $I^{-1}$  in any direction. Directions in stimulus space where the Fisher information has large eigenvalues permit precise estimation; directions where the eigenvalues are small produce large estimation noise.

Now consider an ideal observer who must decide whether the stimulus is  $\mathbf{s}$  (no change) or  $\mathbf{s} + \Delta\mathbf{s}$  (a small shift). Under the null hypothesis the stimulus estimate is distributed approximately as  $\hat{\mathbf{s}} \sim \mathcal{N}(\mathbf{s}, I^{-1})$ , and under the alternative as  $\hat{\mathbf{s}} \sim \mathcal{N}(\mathbf{s} + \Delta\mathbf{s}, I^{-1})$ . These are two multivariate Gaussians with the same covariance but shifted means. The optimal discriminability between them is the Mahalanobis distance of the mean shift measured in the inverse covariance of the noise:

$$(d')^2 = \Delta\mathbf{s}^T (I^{-1})^{-1} \Delta\mathbf{s} = \Delta\mathbf{s}^T I(\mathbf{s}) \Delta\mathbf{s}. \quad (8)$$

This is a standard result in signal detection theory [7]: for two Gaussians with shared covariance  $\Sigma$ , the detection sensitivity is  $d'^2 = \Delta\boldsymbol{\mu}^T \Sigma^{-1} \Delta\boldsymbol{\mu}$ , and here  $\Sigma = I^{-1}$  so  $\Sigma^{-1} = I$ .

Threshold corresponds to a fixed criterion  $d' = c$ , giving the set of just-detectable shifts as

$$\{\Delta\mathbf{s} : \Delta\mathbf{s}^T I \Delta\mathbf{s} = c^2\},$$

which is an ellipsoid in stimulus space with shape matrix  $\Sigma = c^2 I^{-1}$ . The semi-axes of this ellipsoid are  $c/\sqrt{\mu_k}$ , where  $\mu_k$  are the eigenvalues of  $I$ .

This is the geometric meaning of setting  $g = I$ : the Fisher information matrix defines a Riemannian metric, and discrimination thresholds trace out the unit ball of the inverse metric. The criterion constant  $c$  is a global scale factor that depends on the experimental procedure (e.g., the target percent correct in a forced-choice task) and is absorbed by the STRESS optimal scale factor  $F$  when comparing with data.

### 4.3 Directional tuning and the rank-1 structure

V1 neurons respond selectively to chromatic direction. A neuron tuned to a preferred direction  $\hat{\mathbf{n}} = (\cos\theta, \sin\theta)$  in the  $(z, w)$  plane has a firing rate that depends on the stimulus only through the scalar projection onto  $\hat{\mathbf{n}}$ :

$$f(\mathbf{s}) = \phi(\hat{\mathbf{n}} \cdot \mathbf{s}), \quad (9)$$

where  $\phi$  is the neuron's (generally nonlinear) contrast-response function. Taking partial derivatives by the chain rule,

$$\frac{\partial f}{\partial s_i} = \phi'(\hat{\mathbf{n}} \cdot \mathbf{s}) \hat{n}_i,$$

so the gradient  $\nabla f = \phi' \hat{\mathbf{n}}$ . Substituting into (6) gives

$$I = \frac{[\phi']^2}{\phi} \hat{\mathbf{n}} \hat{\mathbf{n}}^T. \quad (10)$$

Note that any single Poisson neuron has rank-1 Fisher information, since  $I = f^{-1} \nabla f \nabla f^T$  is always an outer product regardless of tuning shape. The directional tuning assumption (9) determines the *direction* of this rank-1 contribution: it is aligned with the neuron's preferred chromatic direction  $\hat{\mathbf{n}}$ . The scalar prefactor  $[\phi']^2/\phi$  depends on the neuron's gain and operating point but the geometric structure (the outer product  $\hat{\mathbf{n}} \hat{\mathbf{n}}^T$ ) depends only on the preferred direction.

### 4.4 Population additivity

Fisher information is additive across conditionally independent neurons (independent spike counts given the stimulus) [4]. Cortical neurons do exhibit noise correlations, but for populations with shared tuning the dominant effect of correlations is to rescale the aggregate Fisher information rather than change its directional structure [7]. If a population of  $N_k$  neurons shares preferred direction  $\hat{\mathbf{n}}_k$  and has aggregate scalar Fisher information  $\lambda_k$  (absorbing population size, per-neuron gain, and operating point), then the total Fisher information of the population is

$$I_{\text{pop}} = \sum_k \lambda_k \hat{\mathbf{n}}_k \hat{\mathbf{n}}_k^T. \quad (11)$$

For a metric tensor, the key requirement is that this matrix be positive definite, which holds whenever the set of preferred directions  $\{\hat{\mathbf{n}}_k\}$  spans  $\mathbb{R}^2$  (i.e., not all neurons are tuned to the same direction).

### 4.5 Three V1 sub-populations

Electrophysiological recordings show that V1 neurons span a continuum of chromatic preferences, but with clustering near the cardinal axes and a broad distribution of intermediate (non-cardinal) tunings [21, 13, 14]. We model this distribution as three discrete sub-populations:

- (i) *Parvocellular-recipient neurons*, tuned along the L-M axis ( $\hat{\mathbf{n}} = \mathbf{e}_z$ ). Their aggregate Fisher information is  $\lambda_P \mathbf{e}_z \mathbf{e}_z^T$ .

- (ii) *Koniocellular-recipient neurons*, tuned along the S-cone axis ( $\hat{\mathbf{n}} = \mathbf{e}_w$ ). Their aggregate Fisher information is  $\lambda_K \mathbf{e}_w \mathbf{e}_w^T$ , where  $\lambda_K$  differs from  $\lambda_P$  because the koniocellular pathway has fewer neurons and different contrast gain [10, 32]. We write  $\lambda_K = \gamma^2 \mathcal{N}(z)$ , where  $\gamma$  captures the baseline sensitivity ratio and  $\mathcal{N}(z)$  is a cross-channel normalization factor (see 4.7).
- (iii) *Non-cardinal neurons*, tuned to a chromaticity-dependent intermediate direction  $\hat{\mathbf{n}}(\theta)$  where  $\theta = \theta(z, w)$ . Their aggregate Fisher information is  $\lambda_N \hat{\mathbf{n}} \hat{\mathbf{n}}^T$ , where  $\lambda_N = \eta^2 \mathcal{S}(w)$  incorporates both the population weight  $\eta^2$  and an S-cone disinhibition factor  $\mathcal{S}(w)$  (Section 4.8).

Applying (11) with these three populations gives the combined Fisher information at fixed luminance:

$$G_0(z, w) = \lambda_P \mathbf{e}_z \mathbf{e}_z^T + \gamma^2 \mathcal{N}(z) \mathbf{e}_w \mathbf{e}_w^T + \eta^2 \mathcal{S}(w) \hat{\mathbf{n}} \hat{\mathbf{n}}^T. \quad (12)$$

Since  $\mathbf{e}_z$  and  $\mathbf{e}_w$  are orthogonal and both carry strictly positive coefficients, the first two terms alone form a positive definite diagonal matrix, and the non-cardinal term (which is positive semi-definite) can only increase the eigenvalues. The matrix is therefore positive definite for all values of  $\theta$  and all  $\eta \geq 0$ .

Because only ratios of the population weights are observable in threshold data (STRESS normalizes by an optimal global scale factor), we set  $\lambda_P = 1$  without loss of generality. The parameters  $\gamma$  and  $\eta$  then measure konio and non-cardinal sensitivity relative to the parvocellular population.

## 4.6 Luminance scaling

The aggregate scalar Fisher information  $\lambda_k$  of each population depends on luminance through the firing rates of its neurons. If firing rates scale as a power law of luminance,  $f(\mathbf{s}; Y) = c(\mathbf{s}) Y^a$ , then the Poisson Fisher information (6) becomes

$$I_{ij}(\mathbf{s}; Y) = \frac{1}{c Y^a} \frac{\partial(c Y^a)}{\partial s_i} \frac{\partial(c Y^a)}{\partial s_j} = \frac{[c'_i][c'_j]}{c} Y^a, \quad (13)$$

where  $c'_i = \partial c / \partial s_i$ . The  $Y^{2a}$  from the numerator partially cancels the  $Y^a$  in the denominator (the Poisson variance), leaving a net scaling of  $Y^a$ . When  $a = 0$  the chromatic Fisher information is luminance-independent, meaning the von Kries adaptation in the earlier stages has fully normalized the luminance dependence.

Different pathways have different luminance-response exponents [16, 12]. Writing  $a_P$  for the parvo exponent and  $a_K$  for the konio exponent, the luminance-dependent Fisher information of each population factorizes as  $\lambda_k(z, w) \cdot Y^{a_k}$ . We absorb the chromaticity-dependent scalar  $\lambda_k(z, w)$  into the population parameters (with  $\lambda_P = 1$  by the normalization convention above), giving the full metric

$$G(z, w; Y) = G_P + G_K + G_N, \quad (14)$$

where

$$G_P = Y^{a_P} \mathbf{e}_z \mathbf{e}_z^T, \quad (15)$$

$$G_K = \mathcal{N}(z) \gamma^2 Y^{a_K} \mathbf{e}_w \mathbf{e}_w^T, \quad (16)$$

$$G_N = \eta^2 \mathcal{S}(w) Y^{(a_P + a_K)/2} \hat{\mathbf{n}} \hat{\mathbf{n}}^T. \quad (17)$$

The parvo and konio terms each carry their own luminance exponent. The non-cardinal term uses  $Y^{(a_P+a_K)/2}$ , the geometric mean of the two pathway exponents. This is a modeling choice reflecting the convergent input that non-cardinal V1 neurons receive from both the parvocellular and koniocellular streams; we do not have direct measurements of a separate non-cardinal luminance exponent, so we treat it as intermediate between the two pathways it draws from.

## 4.7 Cross-channel normalization

The two normalization factors  $\mathcal{N}(z)$  and  $\mathcal{S}(w)$  implement cross-channel gain control within the Fisher information framework. The konio cross-normalization factor

$$\mathcal{N}(z) = \frac{\tau}{\tau + z^2} \quad (18)$$

suppresses koniocellular sensitivity at chromaticities with high L-M opponent activity ( $|z| \gg 0$ ). This is a form of Carandini–Heeger divisive normalization [3] applied to the chromatic domain: the normalization pool consists of L-M opponent activity in the parvocellular surround, which suppresses the S-cone pathway response. Solomon, Peirce & Lennie [38] measured precisely this type of cross-mechanism suppression in macaque V1, finding that L-M gratings reduce the responses of S-cone-driven neurons.

At the adaptation white ( $z \approx 0$ ),  $\mathcal{N} \approx 1$  and the konio channel operates at full sensitivity. At spectrum-locus chromaticities with strong L-M contrast ( $z^2 \gg \tau$ ),  $\mathcal{N} \rightarrow 0$  and the konio channel is suppressed.

The S-cone disinhibition factor

$$\mathcal{S}(w) = 1 + \frac{\delta_{\text{nc}} \sigma_w^2}{w^2 + \sigma_w^2} \quad (19)$$

modulates the non-cardinal population in the opposite sense: it boosts non-cardinal sensitivity when S-cone input is absent. The neurophysiological basis and geometric consequences of this factor are described in Section 4.8.

The non-cardinal preferred direction varies across the chromaticity plane as a linear function of the opponent coordinates:

$$\theta(z, w) = \theta_0 + \theta_1 z + \theta_2 (w - w_0), \quad w_0 = \frac{(0.5)^{p_s}}{(0.5)^{p_s} + \kappa_s}. \quad (20)$$

Here  $w_0$  is the koniocellular coordinate at the adaptation white ( $r = 0.5$  when all adapted cone signals equal unity). The linear field is the simplest parameterization that allows ellipse orientations to vary across the chromaticity diagram.

**Proposition 4.1** (Positive definiteness).  *$G(z, w; Y)$  as defined in (14) is positive definite for all  $Y > 0$ ,  $\gamma > 0$ ,  $\tau > 0$ ,  $\delta_{\text{nc}} \geq 0$ ,  $\sigma_w > 0$ , and  $\eta \geq 0$ .*

*Proof.* Since  $\tau > 0$  and  $z^2 \geq 0$ , we have  $0 < \mathcal{N} \leq 1$ . The diagonal matrix  $\text{diag}(Y^{a_P}, \mathcal{N} \gamma^2 Y^{a_K})$  therefore has strictly positive entries for  $Y > 0$  and  $\gamma > 0$ , hence is positive definite. Since  $\delta_{\text{nc}} \geq 0$  and  $\sigma_w > 0$ , we have  $\mathcal{S}(w) \geq 1 > 0$ . The rank-1 matrix  $\eta^2 \mathcal{S}(w) Y^{(a_P+a_K)/2} \hat{\mathbf{n}} \hat{\mathbf{n}}^T$  is positive semi-definite (its eigenvalues are 0 and  $\eta^2 \mathcal{S} Y^{(a_P+a_K)/2} \geq 0$ ). The sum of a positive definite matrix and a positive semi-definite matrix is positive definite.  $\square$

## 4.8 S-cone disinhibition of the non-cardinal population

The non-cardinal V1 population receives convergent input from both parvocellular and koniocellular pathways. Solomon, Peirce & Lennie [38] measured cross-mechanism suppression in macaque V1 and found that S-cone signals modulate the responses of non-cardinal chromatic neurons: S-cone activity suppresses the sensitivity of neurons tuned to intermediate chromatic directions.

When S-cone input is absent, this suppression is released. On the spectrum locus above approximately 510 nm, the S-cone fundamental sensitivity is negligible, so the koniocellular opponent coordinate  $w$  approaches zero.

The S-cone disinhibition factor (19) resolves this tradeoff. When  $w \rightarrow 0$  (no S-cone signal),  $\mathcal{S} \approx 1 + \delta_{\text{nc}}$ , boosting non-cardinal sensitivity by a factor of  $1 + \delta_{\text{nc}}$ . At the adaptation white ( $w = w_0 \approx 6\sigma_w$  for the fitted parameters),  $\mathcal{S} \approx 1.27$ , a modest residual boost. At chromaticities with high S-cone content ( $w \gg w_0$ ),  $\mathcal{S} \rightarrow 1$ . The ratio of the disinhibition at S-cone-absent wavelengths to its value at the adaptation white is approximately  $(1 + \delta_{\text{nc}})/\mathcal{S}(w_0) \approx 9$ , providing strong differential sensitivity.

The important geometric property is that the koniocellular coordinate  $w$  separates the Wright problem wavelengths from the MacAdam centres. At Wright 520–560 nm,  $w/w_0$  ranges from approximately 0.03 to 0.23 while at all 25 MacAdam centres,  $w/w_0$  is substantially larger because broadband stimuli inside the gamut retain measurable S-cone excitation even at red and green chromaticities. This separation is a consequence of the spectrum locus having negligible S-cone content above 510 nm, while all broadband stimuli retain measurable S-cone excitation. No other opponent coordinate provides comparable separation.

## 5 The Metric

### 5.1 Pullback to chromaticity coordinates

The opponent coordinate map  $\Phi: (x, y) \mapsto (z, w)$  at fixed luminance  $Y$  has a  $2 \times 2$  Jacobian

$$J_{\text{opp}} = \frac{\partial(z, w)}{\partial(x, y)}, \quad (21)$$

computed numerically by central differences. The Riemannian metric on the chromaticity plane, expressed in CIE  $(x, y)$  coordinates, is the pullback:

$$g_{\text{chrom}}(x, y; Y) = J_{\text{opp}}^T G(z, w; Y) J_{\text{opp}}. \quad (22)$$

### 5.2 Luminance metric: Magnocellular pathway

Luminance discrimination is mediated primarily by the magnocellular pathway, which receives additive  $L + M$  input and has high contrast sensitivity [16, 26]. We derive the luminance metric from the same Poisson Fisher information framework used for the chromatic channels.

A magnocellular neuron encoding luminance has a firing rate that depends on  $Y$  through a power law  $f(Y) = cY^{a_M}$ , where  $a_M$  is the magnocellular luminance-response exponent and  $c$  absorbs the neuron’s baseline sensitivity. The one-dimensional Poisson Fisher information for the parameter  $Y$  is

$$g_{YY}^{(\text{single})} = \frac{[f'(Y)]^2}{f(Y)} = \frac{[c a_M Y^{a_M-1}]^2}{c Y^{a_M}} = c a_M^2 Y^{a_M-2}.$$

Summing over a population of magnocellular neurons (as in Section 4.6) gives an aggregate Fisher information

$$g_{YY}(Y) = \lambda_M Y^{a_M-2}, \quad (23)$$

where  $\lambda_M$  absorbs the population size and per-neuron parameters.

It is convenient to reparameterize by defining  $\beta_Y = (2 - a_M)/2$ , so that  $a_M = 2(1 - \beta_Y)$  and  $a_M - 2 = -2\beta_Y$ . Then (23) becomes

$$g_{YY}(Y) = \psi_0^2 / Y^{2\beta_Y}, \quad (24)$$

where  $\psi_0^2 = \lambda_M$  absorbs the population-level prefactor. The reparameterization is natural because  $\beta_Y$  directly governs the power law of luminance discrimination thresholds: since  $\Delta Y \propto 1/\sqrt{g_{YY}} \propto Y^{\beta_Y}$ , a larger  $\beta_Y$  means thresholds grow faster with luminance.

The two classical limiting cases correspond to specific values of the magnocellular response exponent. When  $a_M = 1$  (linear response),  $\beta_Y = 0.5$  and  $\Delta Y \propto Y^{0.5}$ , which is the de Vries–Rose law characteristic of photon-noise-limited detection. As  $a_M \rightarrow 0$  (nearly constant response),  $\beta_Y \rightarrow 1$  and  $\Delta Y \propto Y$ , approaching Weber’s law for luminance ( $\Delta Y/Y \approx \text{const}$ ), established since König & Brodhun [18]. The fitted value  $\beta_Y = 0.84$  corresponds to  $a_M = 0.32$ , a mildly sublinear magnocellular response: luminance discrimination is closer to Weber’s law than to de Vries–Rose, consistent with the psychophysical literature at moderate photopic luminances [11]. Note that exact Weber’s law ( $\beta_Y = 1$  exactly) would require  $a_M = 0$ , making  $g_{YY}$  identically zero in the Poisson model. The fact that the fitted  $\beta_Y$  falls short of unity is therefore not merely an empirical observation but a structural prediction of the Poisson framework: the magnocellular pathway must retain some luminance dependence in its firing rates for the Fisher information to be nonzero.

### 5.3 The full three-dimensional metric

The chromaticity and luminance metrics are assumed to be block diagonal:

$$g(x, y, Y) = \begin{pmatrix} g_{\text{chrom}}(x, y; Y) & \mathbf{0} \\ \mathbf{0}^T & g_{YY}(Y) \end{pmatrix}. \quad (25)$$

This corresponds to the assumption that the chromatic (parvo/konio) and luminance (magn) pathways contribute independently to the Fisher information. Krauskopf, Williams & Heeley [19] showed that the cardinal directions of color space (L-M, S, and L+M) are approximately independent mechanisms.

The Koenderink et al. [17] data provide a quantitative test of this independence. Each Koenderink ellipsoid is a  $3 \times 3$  covariance matrix  $\Sigma$  in sRGB coordinates. To assess

chromaticity-luminance coupling, we rotate each  $\Sigma$  into a basis where one axis is the achromatic direction  $\mathbf{a} = (1, 1, 1)/\sqrt{3}$  (equal increments in R, G, B correspond to a pure luminance change) and the other two axes span the chromatic plane perpendicular to  $\mathbf{a}$ . In this basis, the  $3 \times 3$  covariance decomposes into a  $2 \times 2$  chromatic block, a  $1 \times 1$  luminance entry, and  $2 \times 1$  cross terms. If the block-diagonal assumption holds exactly, the cross terms vanish. In practice, the ratio of the cross-term magnitudes to the geometric mean of the corresponding diagonal entries ranges from 0.01 to 0.22 at the five achromatic reference colours confirming that the coupling is small but nonzero.

## 6 Parameters

The model has 17 free parameters, each with a neurophysiological origin:

#	Symbol	Neurophysiological origin	Fitted value
0	$p_s$	S-cone transduction exponent	0.597
1	$\kappa_s$	S-cone half-saturation	8.616
2	$\gamma$	Konio/parvo sensitivity ratio	12.85
3	$\eta$	Non-cardinal V1 sensitivity	2.355
4	$\theta_0$	Mean non-cardinal direction	-2.244
5	$\theta_1$	Direction gradient along $z$	0.994
6	$\theta_2$	Direction gradient along $w$	1.508
7	$z_{\max}$	L-M saturation ceiling	1.993
8	$p_z$	L-M Naka–Rushton exponent	1.022
9	$\kappa_z$	L-M half-saturation	1.393
10	$a_P$	Parvo luminance exponent	0.717
11	$a_K$	Konio luminance exponent	0.568
12	$\psi_0$	Magnocellular Weber fraction	0.738
13	$\beta_Y$	Magno luminance exponent	0.841
14	$\tau$	Konio cross-normalization	0.796
15	$\delta_{\text{nc}}$	S-cone disinhibition strength	10.00
16	$\sigma_w$	Disinhibition half-saturation	0.012

The fitted values are from joint optimization across four datasets (Section 8). Parameters 0–9 govern the chromaticity metric. Parameters 10–11 control how the chromatic metric scales with luminance. Parameters 12–13 are constrained only by three-dimensional data. Parameter 14 controls the divisive normalization of the koniocellular channel by parvocellular activity. Parameters 15–16 control the S-cone disinhibition of the non-cardinal population.

## 7 Computing the Discrimination Ellipsoid

This section collects all the pieces into a single recipe. Given a color stimulus with CIE coordinates  $(x, y, Y)$  and an adaptation white with cone signals  $(L_W, M_W, S_W)$ , the following steps produce the predicted  $3 \times 3$  discrimination ellipsoid in any desired coordinate system.

*Step 1. Cone signals and adaptation.* Compute the tristimulus values  $X = Yx/y$ ,  $Z = Y(1-x-y)/y$ , then the cone signals  $(L, M, S) = M_{\text{SP}}(X, Y, Z)^T$  using (1). Di-

vide by the adaptation white:  $L_a = L/L_W$ ,  $M_a = M/M_W$ ,  $S_a = S/S_W$ .

*Step 2. Opponent coordinates.* Compute the two chromaticity coordinates. For the L-M channel, apply the saturating Naka–Rushton to the log cone ratio:

$$u = \log(L_a/M_a), \quad z = z_{\max} \operatorname{sign}(u) \frac{|u|^{p_z}}{|u|^{p_z} + \kappa_z}.$$

For the S channel:

$$r = \frac{S_a}{L_a + M_a}, \quad w = \frac{r^{p_s}}{r^{p_s} + \kappa_s}.$$

These depend only on chromaticity, not on luminance (Proposition 3.1).

*Step 3. Non-cardinal direction.* Compute the preferred direction of the non-cardinal V1 population:

$$\theta = \theta_0 + \theta_1 z + \theta_2 (w - w_0), \quad w_0 = \frac{(0.5)^{p_s}}{(0.5)^{p_s} + \kappa_s}, \quad \hat{\mathbf{n}} = \begin{pmatrix} \cos \theta \\ \sin \theta \end{pmatrix}.$$

*Step 4. Channel metric.* Compute the konio cross-channel normalization factor:

$$\mathcal{N} = \frac{\tau}{\tau + z^2}.$$

Compute the S-cone disinhibition factor:

$$\mathcal{S} = 1 + \frac{\delta_{\text{nc}} \sigma_w^2}{w^2 + \sigma_w^2}.$$

Assemble the  $2 \times 2$  Fisher information matrix in opponent coordinates:

$$G = G_P + G_K + G_N = \begin{pmatrix} Y^{a_P} & 0 \\ 0 & \mathcal{N} \gamma^2 Y^{a_K} \end{pmatrix} + \eta^2 \mathcal{S} Y^{(a_P + a_K)/2} \hat{\mathbf{n}} \hat{\mathbf{n}}^T.$$

The diagonal terms represent the parvocellular and koniocellular populations, with konio sensitivity reduced by  $\mathcal{N}$  at chromaticities with high L-M opponent activity. The rank-1 term represents the non-cardinal population, with sensitivity modulated by  $\mathcal{S}$ : strongly boosted when the S-cone pathway is inactive ( $w \approx 0$ ) and only modestly boosted when S-cone input is present ( $w \gg \sigma_w$ ).

*Step 5. Jacobian.* Compute the  $2 \times 2$  Jacobian  $J_{\text{opp}} = \partial(z, w)/\partial(x, y)$  by repeating Steps 1–2 at four neighboring chromaticities and using central differences:

$$[J_{\text{opp}}]_{i1} = \frac{\Phi_i(x+h, y) - \Phi_i(x-h, y)}{2h}, \quad [J_{\text{opp}}]_{i2} = \frac{\Phi_i(x, y+h) - \Phi_i(x, y-h)}{2h},$$

where  $\Phi = (z, w)$  and  $h \approx 10^{-7}$ .

*Step 6. Chromaticity metric.* Pull the channel metric back to CIE coordinates:

$$g_{\text{chrom}} = J_{\text{opp}}^T G J_{\text{opp}}.$$

This is a  $2 \times 2$  positive definite matrix whose inverse gives the discrimination ellipse at luminance  $Y$ .

*Step 7. Luminance metric.* Compute the scalar luminance metric:

$$g_{YY} = \psi_0^2 / Y^{2\beta_Y}.$$

*Step 8. Full 3D metric.* Assemble the block-diagonal  $3 \times 3$  metric in  $(x, y, Y)$  coordinates:

$$g = \begin{pmatrix} g_{\text{chrom}} & \mathbf{0} \\ \mathbf{0}^T & g_{YY} \end{pmatrix}.$$

*Step 9 (if needed). Coordinate transform.* If the data are in display coordinates  $(R_\gamma, G_\gamma, B_\gamma)$  rather than  $(x, y, Y)$ , compute the  $3 \times 3$  Jacobian  $J_{\text{full}} = \partial(x, y, Y) / \partial(R_\gamma, G_\gamma, B_\gamma)$  by central differences on the display model, then transform:

$$g_{\text{RGB}} = J_{\text{full}}^T g J_{\text{full}}.$$

*Step 10. Output.* The predicted discrimination ellipsoid is  $\Sigma = g_{\text{RGB}}^{-1}$  (or  $g^{-1}$  if working in  $(x, y, Y)$ ), up to the criterion constant  $c^2$  that is absorbed by the STRESS scale factor (Section 4). The eigenvectors of  $\Sigma$  give the principal axes of the ellipsoid; the square roots of the eigenvalues give the semi-axis lengths. For a 2D chromaticity ellipse at fixed  $Y$ , use  $g_{\text{chrom}}^{-1}$  from Step 6.

The entire computation requires only matrix multiplication, one logarithm, one power function, and numerical differentiation. No iterative solvers or special functions are needed.

## 8 Empirical Validation

### 8.1 Datasets

We test the model against four datasets that span threshold discrimination at varied chromaticities, luminances, and stimulus conditions:

- (i) *MacAdam (1942)* [25]: 25 threshold discrimination ellipses, single observer (PGN), constant luminance  $Y = 48 \text{ cd/m}^2$ , Illuminant C adaptation. Data from Wyszecki & Stiles [35].
- (ii) *Koenderink et al. (2026)* [17]: 35 three-dimensional ellipsoids (Notable Qualitative Differences), 8 observers (group median),  $Y = 7.1\text{--}129.2 \text{ cd/m}^2$ , D65 adaptation.
- (iii) *Wright (1941)* [36]: 19 wavelength discrimination thresholds ( $\Delta\lambda$  at threshold) along the spectrum locus from 440–620 nm, single observer,  $Y = 48 \text{ cd/m}^2$ , Illuminant C adaptation.

- (iv) *Huang et al. (2012)* [37]: 17 chromaticity discrimination ellipses at the CIE-recommended colour centres, 16 observers, pass/fail threshold method, printed samples under D65, CIE 1964 10° observer. The centres span luminances  $Y = 9.4\text{--}69.0$  cd/m<sup>2</sup> and chromaticities from near-neutral to high chroma.

## 8.2 Coordinate transformations

The model produces a  $2 \times 2$  chromaticity metric  $g_{\text{chrom}}(x, y; Y)$  in CIE  $(x, y)$  coordinates and a  $3 \times 3$  metric  $g(x, y, Y)$  in CIE  $(x, y, Y)$  coordinates. Each dataset reports discrimination data in a different coordinate system. For each dataset we choose whichever transformation direction avoids numerical instability: the observed data are transformed to CIE  $xy$  where possible, and the model is transformed to the data’s native coordinates where necessary. In all cases the predicted and observed quantities are compared in the same coordinate system. The transformations are as follows.

*MacAdam.* The data are already in CIE  $(x, y)$  coordinates. Each ellipse is specified by semi-axes  $(a, b)$  and orientation  $\vartheta$ , which define an observed  $2 \times 2$  metric tensor directly:

$$g_{\text{obs}} = R(\vartheta) \text{diag}(1/a^2, 1/b^2) R(\vartheta)^T,$$

where  $R(\vartheta)$  is a rotation matrix. No coordinate transformation is needed; the model’s  $g_{\text{chrom}}$  is compared directly with  $g_{\text{obs}}$  at each ellipse centre.

*Koenderink.* The data are  $3 \times 3$  covariance matrices  $\Sigma_{\text{obs}}$  in gamma-encoded sRGB coordinates. The comparison is performed in sRGB: the model’s metric is transformed to sRGB via the  $3 \times 3$  Jacobian

$$J_{\text{full}} = \frac{\partial(x, y, Y)}{\partial(R_\gamma, G_\gamma, B_\gamma)}$$

computed by central differences ( $h = 10^{-7}$ ) through the sRGB display model (gamma decoding followed by the  $3 \times 3$  sRGB-to-XYZ matrix at the display’s peak luminance  $Y_{\text{white}} = 214$  cd/m<sup>2</sup>). The predicted covariance in sRGB is then

$$\Sigma_{\text{pred}} = (J_{\text{full}}^T g J_{\text{full}})^{-1}.$$

Equivalently, one could transform  $\Sigma_{\text{obs}}$  to  $(x, y, Y)$  via  $J_{\text{full}} \Sigma_{\text{obs}} J_{\text{full}}^T$  and compare with  $g^{-1}$ ; the two approaches are related by a change of basis and yield the same STRESS. Predicted and observed covariances are compared along 26 probe directions.

*Wright.* The data are scalar wavelength thresholds  $\Delta\lambda$  at 19 points along the spectrum locus. The chromaticity coordinates  $(x(\lambda), y(\lambda))$  and their gradients  $\mathbf{v}(\lambda) = (\partial x/\partial\lambda, \partial y/\partial\lambda)$  were computed from the CIE 1931 2° colour matching functions at 0.5 nm spacing using central differences. The model predicts a threshold proportional to the inverse of the metric’s sensitivity along the wavelength direction:

$$\Delta\lambda_{\text{pred}} \propto \frac{1}{\sqrt{\mathbf{v}^T g_{\text{chrom}} \mathbf{v}}}.$$

The proportionality constant (which depends on the observer’s criterion) is absorbed by the optimal scaling factor  $F$  in STRESS.

*Huang.* The data are ellipses in the CIELAB  $a_{10}^* b_{10}^*$  plane (10° observer, D65 white). Each ellipse is specified by a semi-major axis  $A$ , an axis ratio  $A/B$ , and an orientation  $\vartheta$ . These define an observed metric tensor in  $(a^*, b^*)$  coordinates:

$$g_{a^*b^*} = R(\vartheta) \text{diag}(1/A^2, 1/B^2) R(\vartheta)^T.$$

To transform into CIE  $(x, y)$  we compute the  $2 \times 2$  Jacobian  $J_{ab} = \partial(a_{10}^*, b_{10}^*)/\partial(x, y)$  numerically ( $h = 10^{-5}$ ) by perturbing  $(x, y)$  at fixed  $Y$  and passing through the CIELAB forward equations with the 10° D65 white point  $(X_n, Y_n, Z_n) = (94.811, 100.0, 107.304)$ . The observed metric in  $(x, y)$  coordinates is then

$$g_{\text{obs}} = J_{ab}^T g_{a^*b^*} J_{ab},$$

which is compared with  $g_{\text{chrom}}$  evaluated at the colour centre. Note that the model uses 2° cone fundamentals throughout which creates small errors in our predictions for this dataset

### 8.3 Evaluation measures

*STRESS* (Standardized Residual Sum of Squares) compares predicted and observed ellipse radii at multiple probe directions, with an optimal global scaling factor  $F$ :

$$\text{STRESS} = 100 \sqrt{\frac{\sum_i (r_i - F p_i)^2}{\sum_i r_i^2}} \quad (26)$$

where  $r_i$  and  $p_i$  are observed and predicted radii in probe direction  $i$ .

### 8.4 Results

The Fisher Information model, with a single set of 17 parameters fitted jointly to four datasets, is the only model that achieves competitive performance across all datasets simultaneously.

On MacAdam it achieves STRESS of 23.9 versus 30.2 for the best standard model (CIECAM02-UCS [24]), a 21% improvement (Figure 3). On Koenderink it achieves STRESS of 20.8 (Figure 2).

On Wright wavelength discrimination, the Fisher Information model achieves STRESS of 30.1 versus 58.8 for the best standard model (CIECAM02-UCS), a 49% improvement. All standard metrics cluster at STRESS 58–63 on this dataset because none possess a mechanism for the large sensitivity variations along the spectrum locus. Two normalization mechanisms contribute to this improvement. The konio cross-normalization factor  $\mathcal{N}$  suppresses the S-cone pathway at chromaticities with high L-M opponent activity: at blue-green wavelengths around 470–500 nm, the substantial L-M opponent contrast reduces  $\mathcal{N}$  well below unity, suppressing the excess konio sensitivity that otherwise predicts thresholds well below Wright’s observations. The S-cone disinhibition factor  $\mathcal{S}$  boosts non-cardinal sensitivity at chromaticities where the S-cone pathway is inactive.

Dataset	Model	STRESS
MacAdam	CIELAB	41.9
MacAdam	CIEDE2000	37.6
MacAdam	CIECAM02-UCS	30.2
MacAdam	CAM16-UCS	30.5
MacAdam	Fisher Information	23.9
Koenderink et al.	CIELAB	26.2
Koenderink et al.	CIEDE2000	25.2
Koenderink et al.	CIECAM02-UCS	28.1
Koenderink et al.	CAM16-UCS	29.2
Koenderink et al.	Fisher Information	20.8
Wright	CIELAB	61.3
Wright	CIEDE2000	59.3
Wright	CIECAM02-UCS	58.8
Wright	CAM16-UCS	62.6
Wright	Fisher Information	30.1
Huang et al.	CIELAB	35.8
Huang et al.	CIEDE2000	30.7
Huang et al.	CIECAM02-UCS	28.8
Huang et al.	CAM16-UCS	26.1
Huang et al.	Fisher Information	30.8

Table 1: Performance across four datasets. Fisher Information is the 17-parameter model optimized simultaneously across all four datasets with weights  $1.5\times$  MacAdam,  $1.0\times$  Koenderink,  $1.0\times$  Wright,  $0.75\times$  Huang.

On the Huang et al. threshold ellipses (Figure 1), the model achieves STRESS of 30.8, comparable to CIEDE2000 (30.7) and better than CIELAB (35.8), though below CAM16-UCS (26.1) on this individual dataset. CAM16-UCS has an advantage on Huang, likely because its chromatic adaptation transform and chroma compression were tuned to suprathreshold data at varied chromaticities that partially overlap with the Huang conditions. However, CAM16-UCS fails on Wright (62.6), demonstrating that no standard metric achieves the cross-dataset balance of the Fisher Information model.

Huang et al. (2012) — observed (blue) vs predicted (red dashed), 5 × mag. STRESS = 30.8

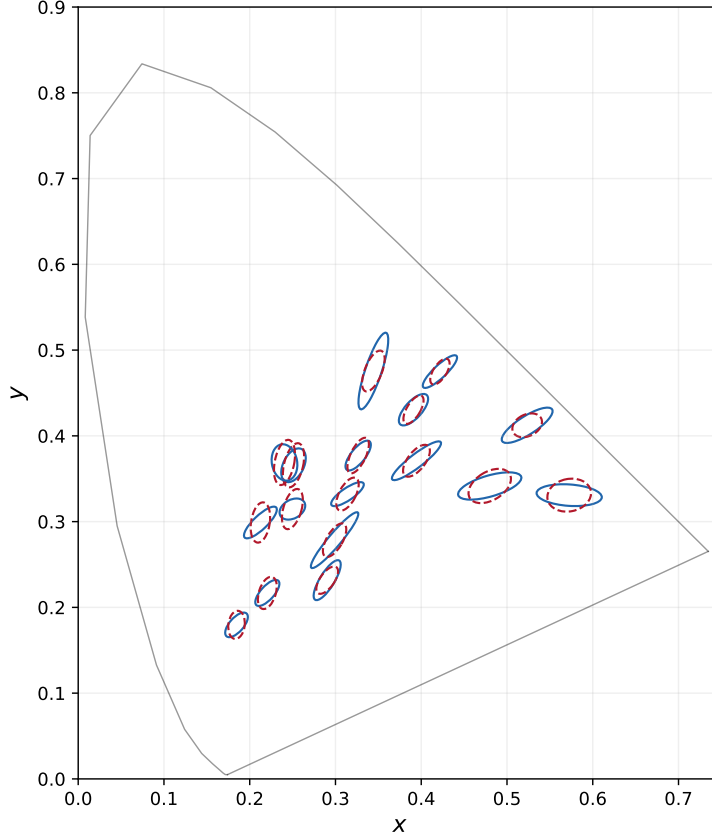


Figure 1: Huang et al. (2012) threshold ellipses: observed (blue, solid) versus predicted (red, dashed) at 5× magnification in CIE  $(x, y)$  coordinates, after transforming the original CIELAB ellipses.

Koenderink et al. (2026) — observed (blue) vs predicted (red dashed), 2.5 × mag. STRESS = 20.8

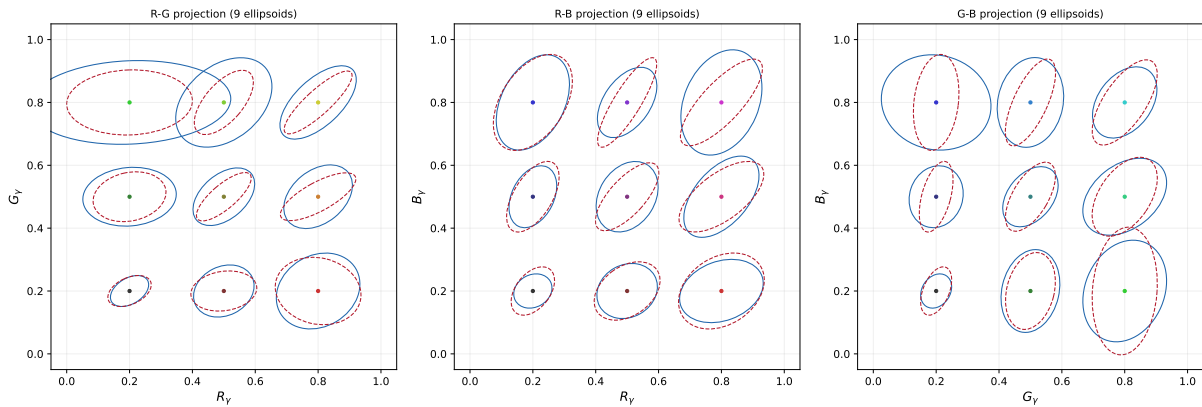


Figure 2: Koenderink et al. (2026) discrimination ellipsoids projected onto three pairs of sRGB coordinates: observed (blue, solid) versus predicted (red, dashed) at 2.5× magnification. A mostly non-overlapping subset of ellipsoids is shown in each panel (number indicated in subtitle); the STRESS-optimal scale factor is computed from all 35 ellipsoids. Centre dots are coloured by sRGB value. STRESS = 20.8.

MacAdam (1942) — observed (blue) vs predicted (red dashed), 10 × mag. STRESS = 23.9

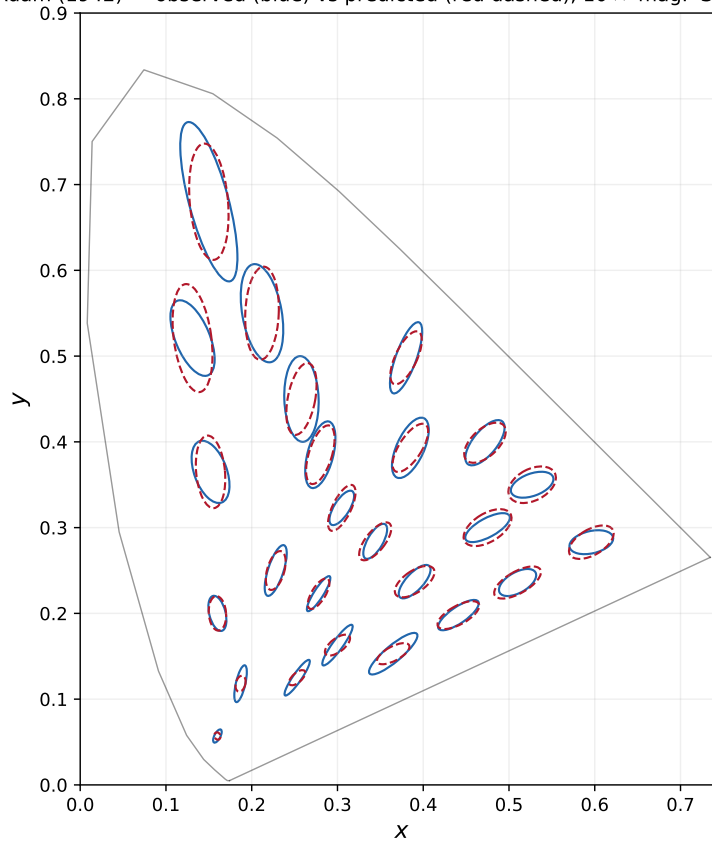


Figure 3: MacAdam (1942) discrimination ellipses: observed (blue, solid) versus predicted (red, dashed) at 10× magnification. The predicted ellipses use the STRESS-optimal global scale factor  $F$ . The model captures ellipse orientations and aspect ratios across the chromaticity diagram. STRESS = 23.9.

## References

- [1] J. K. Bowmaker and H. J. A. Dartnall, *Visual pigments of rods and cones in a human retina*, J. Physiol. **298**, 501–511 (1980).
- [2] D. H. Brainard and B. A. Wandell, *Asymmetric color matching: how color appearance depends on the illuminant*, J. Opt. Soc. Am. A **9**, 1433–1448 (1992).
- [3] M. Carandini and D. J. Heeger, *Normalization as a canonical neural computation*, Nat. Rev. Neurosci. **13**, 51–62 (2012).
- [4] T. M. Cover and J. A. Thomas, *Elements of Information Theory*, 2nd ed. (Wiley, 2006).
- [5] D. M. Dacey and B. B. Lee, *The ‘blue-on’ opponent pathway in primate retina originates from a distinct bistratified ganglion cell type*, Nature **367**, 731–735 (1994).
- [6] D. M. Dacey, *Parallel pathways for spectral coding in primate retina*, Annu. Rev. Neurosci. **23**, 743–775 (2000).
- [7] P. Dayan and L. F. Abbott, *Theoretical Neuroscience: Computational and Mathematical Modeling of Neural Systems* (MIT Press, 2001).
- [8] H. Helson, *Fundamental problems in color vision. I.*, J. Exp. Psychol. **23**, 439–476 (1938).
- [9] H. von Helmholtz, *Versuch einer erweiterten Anwendung des Fechnerschen Gesetzes*, Z. Psychol. Physiol. Sinnesorg. **2**, 1–30 (1891).
- [10] S. H. C. Hendry and R. C. Reid, *The koniocellular pathway in primate vision*, Annu. Rev. Neurosci. **23**, 127–153 (2000).
- [11] D. C. Hood and M. A. Finkelstein, *Sensitivity to light*, in *Handbook of Perception and Human Performance*, Vol. 1, Ch. 5 (1986).
- [12] G. E. Irvin, T. T. Norton, M. A. Sesma, and V. A. Casagrande, *Center/surround relationships of magnocellular, parvocellular, and koniocellular relay cells in primate lateral geniculate nucleus*, Vis. Neurosci. **10**, 363–373 (1993).
- [13] E. N. Johnson, M. J. Hawken, and R. Shapley, *The spatial transformation of color in the primary visual cortex of the macaque monkey*, Nat. Neurosci. **4**, 409–416 (2001).
- [14] E. N. Johnson, M. J. Hawken, and R. Shapley, *Cone inputs in macaque primary visual cortex*, J. Neurophysiol. **91**, 2501–2514 (2004).
- [15] D. B. Judd, *Hue, saturation, and lightness of surface colors with chromatic illumination*, J. Opt. Soc. Am. **30**, 2–32 (1940).
- [16] E. Kaplan and R. M. Shapley, *The primate retina contains two types of ganglion cells, with high and low contrast sensitivity*, Proc. Natl. Acad. Sci. USA **83**, 2755–2757 (1986).
- [17] J. Koenderink, A. van Doorn, D. I. Braun, and K. R. Gegenfurtner, *An empirical three-dimensional metric field for color space*, bioRxiv 2026.03.09.710376 (2026).

- [18] A. König and E. Brodhun, *Experimentelle Untersuchungen über die psychophysische Fundamentalformel*, Sitzungsber. Preuss. Akad. Wiss., 917–931 (1889).
- [19] J. Krauskopf, D. R. Williams, and D. W. Heeley, *Cardinal directions of color space*, Vision Res. **22**, 1123–1131 (1982).
- [20] I. Kuriki, *The locus of achromatic points in a luminance-level effect*, Color Res. Appl. **31**, 204–211 (2006).
- [21] P. Lennie, J. Krauskopf, and G. Sclar, *Chromatic mechanisms in striate cortex of macaque*, J. Neurosci. **10**, 649–669 (1990).
- [22] C. Li et al., *Comprehensive color solutions: CAM16, CAT16, and CAM16-UCS*, Color Res. Appl. **42**, 703–718 (2017).
- [23] M. R. Luo, G. Cui, and B. Rigg, *The development of the CIE 2000 colour-difference formula: CIEDE2000*, Color Res. Appl. **26**, 340–350 (2001).
- [24] M. R. Luo, G. Cui, and C. Li, *Uniform colour spaces based on CIECAM02 colour appearance model*, Color Res. Appl. **31**, 320–330 (2006).
- [25] D. L. MacAdam, *Visual sensitivities to color differences in daylight*, J. Opt. Soc. Am. **32**, 247–274 (1942).
- [26] W. H. Merigan and J. H. R. Maunsell, *How parallel are the primate visual pathways?*, Annu. Rev. Neurosci. **16**, 369–402 (1993).
- [27] K. I. Naka and W. A. H. Rushton, *S-potentials from colour units in the retina of fish (Cyprinidae)*, J. Physiol. **185**, 536–555 (1966).
- [28] D. M. Schneeweis and J. L. Schnapf, *The photovoltage of macaque cone photoreceptors: adaptation, noise, and kinetics*, J. Neurosci. **19**, 1203–1216 (1999).
- [29] E. Schrödinger, *Grundlinien einer Theorie der Farbenmetrik im Tagessehen*, Ann. Phys. **368**, 481–520 (1920).
- [30] V. C. Smith and J. Pokorny, *Spectral sensitivity of the foveal cone photopigments between 400 and 500 nm*, Vision Res. **15**, 161–171 (1975).
- [31] W. S. Stiles, *A modified Helmholtz line-element in brightness-colour space*, Proc. Phys. Soc. **58**, 41 (1946).
- [32] C. Tailby, S. G. Solomon, and P. Lennie, *Functional asymmetries in visual pathways carrying S-cone signals in macaque*, J. Neurosci. **28**, 4078–4087 (2008).
- [33] J. von Kries, *Die Gesichtsempfindungen*, in *Handbuch der Physiologie des Menschen*, Vol. 3 (1905).
- [34] T. Wachtler, T. J. Sejnowski, and T. D. Albright, *Representation of color stimuli in awake macaque primary visual cortex*, Neuron **37**, 681–691 (2003).
- [35] G. Wyszecki and W. S. Stiles, *Color Science: Concepts and Methods, Quantitative Data and Formulae*, 2nd ed., Wiley (2000).

- [36] W. D. Wright, *The sensitivity of the eye to small colour differences*, Proc. Phys. Soc. **53**, 93–112 (1941).
- [37] M. Huang, H. Liu, G. Cui, M. R. Luo, and M. Melgosa, *Evaluation of threshold colour differences using printed samples*, Color Res. Appl. **37**, 41–51 (2012).
- [38] S. G. Solomon, J. W. Peirce, and P. Lennie, *The impact of suppressive surrounds on chromatic properties of cortical neurons*, J. Neurosci. **24**, 148–160 (2004).